ELSEVIER

Journal of Nuclear Materials 249 (1997) 231–238

journal of nuclear materials

A model for hydride-induced embrittlement in zirconium-based alloys

D. Wäppling [a,b], A.R. Massih [a,b,*], P. Ståhle [b]

[a] *ABB Atom AB, S-721 63 Västerås, Sweden*
[b] *Luleå University of Technology, S-971 87 Luleå, Sweden*

Received 14 February 1997; accepted 30 May 1997

Abstract

The critical stress intensity factor for hydrided zirconium-alloys is calculated using a Dugdale type model for a finite crack. The hydride platelets are assumed to surround the ends of the crack. They are located in the process region of the crack tip. The model is used to calculate the temperature dependence of the critical stress intensity factor and the results are compared with measurements performed on Zr–2.5Nb and Zircaloy. The model in general describes the experimental data satisfactorily, nevertheless, it gives implausible results for a certain range of temperatures. The deficiency is attributed to the lack of appropriate constitutive relations for the hydrided zirconium-based alloys. © 1997 Elsevier Science B.V.

1. Introduction

Zirconium-based alloys are widely used in core structural components of water-cooled and water-moderated reactors due to zirconium's low neutron absorption nuclear cross-section in thermal neutron energies. Examples of these components are fuel claddings and spacer grids in light water reactors, fuel channels in boiling water reactors, pressure tubes of CANDU® nuclear reactors, etc.

In light water reactors one of the main obstacles for extending the burnup of the fuel has been extensive hydriding of Zircaloy cladding emanating from the metal water reaction during operation. Because of the technological importance of this phenomenon, hydrogen embrittlement of zirconium alloys has been studied extensively over the last three decades [1–3].

The formation of hydrides in Zr can have detrimental effects to mechanical properties, comprising tensile ductility [1,3], fracture toughness [3], and ultimate fracture strength [4]. These studies show that the amount of ductility degradation depends on hydride orientation, morphology, and distribution. Hydride platelets oriented normal to stress direction have been found to render large reductions in strength and ductility of Zr-alloys, whereas hydride platelets oriented parallel to the stress direction have little effect. When hydride platelets are densely spaced they can cause brittle fracture, but ductile fracture occurs with sparsely spaced hydrides [1]. The conventional wisdom on hydride-induced embrittlement in Zr-alloys is that both the metastable, γ, and the stable, δ, Zr-hydride phases are intrinsically brittle at temperatures less than 150°C [1,5]. When tensile loads are applied at temperatures below 150°C the hydrides that are oriented normal to the direction of stress readily fracture and microcracks form in the hydrides that enhance the main crack propagation through the material. If a hydride is located at the tip of the crack this leads to a tractable path of crack propagation. Densely spaced hydride platelets are more damaging than the sparsely spaced ones because of the shorter distance for microcrack interlinkage. When a continuous hydride network is formed a brittle fracture mechanism in Zr-alloys occurs [6].

The subcritical fracture behavior of hydrided Zr-alloys can be characterized by the threshold (or critical) stress intensity factor in mode I [7]. Simpson and Puls [8] have observed that for sharp cracks, over a certain range of the stress intensity factors K_I, the crack velocity is only weakly dependent on K_I. The threshold intensity factor, K_{Ic}, is defined as the limiting stress intensity value below which the crack velocity becomes vanishingly small. Any

* Corresponding author. Tel.: +46-21 347 609; fax: +46-21 122 946; e-mail: atoalma@ato.abb.se.

PII S0022-3115(97)00183-9

crack subjected to a K_I less than K_{Ic} will not be able to propagate through the material.

In this paper an analytical model for calculating a criterion for crack growth expressed in terms of a critical stress intensity factor is proposed.

A finite crack of mode I, located in an elastic body, is considered. It is assumed that a hydride platelet is located at the end of the crack and the crack propagation takes place through the hydride. The stress field in the hydride in the presence of the crack is calculated using the Dugdale model [9]. Shi and Puls [7], in contrast, considered a semi-finite crack, the tip of which ends at a hydride platelet. They assumed as Banks and Garlick [10] that in the immediate neighborhood of the crack tip the plastic zone size is given by $r_{pz} = b(K_I/\sqrt{2\pi}\sigma_0)^2$ where b is a proportionality constant and σ_0 is the yield stress of the material. Further, Shi and Puls postulated that in that zone the stress remains constant at its maximum value.

The model considered in this paper and the results of model calculations are presented in Section 2. In Section 3 we extend the model to treat the case of multi-hydride platelets.

2. The model

Experiments indicate that zirconium hydrides formed at crack tips are platelets [11]. These platelets lie in, or close to, the crack plane. The purpose of the model developed here is to predict at what applied stresses the crack propagates through the hydride. Let us consider an infinite elastic body containing a crack of length $2a$ under mode I loading located between two hydride platelets each of length L (Fig. 1).

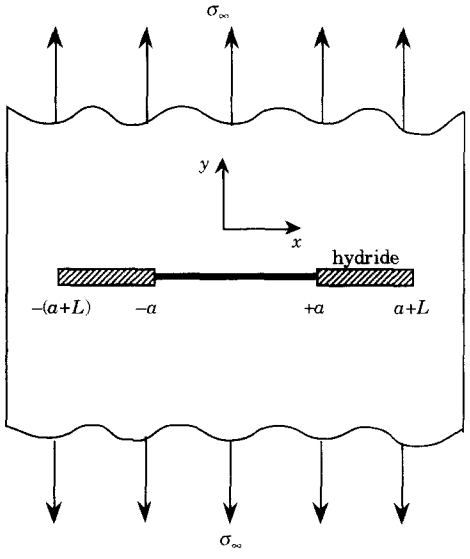

Fig. 1. A body with a crack of length $2a$ contained at both ends with hydride platelets each of length L.

We consider that the hydride platelet of length L covers the *process* zone of length d with $L \geq d$. The process zone is a region characterized by microseparations such as voids or micro-cracks [12]. Under loading, the length of the process region grows, hence increasing the displacement at the crack tip until the limit displacement u^* is attained. At this stage the process region is said to be fully developed, i.e., the crack grows under the constraint $\sigma_{yy}(u > u^*) = 0$, with σ_{yy} being the stress in the y-direction.

The model considered here (Fig. 1) is mathematically described by a boundary value problem in the theory of elasticity. More specifically, a linear elastic semi-infinite body, occupying the upper half plane $y > 0$, is subjected to a remote stress σ_∞ with the following boundary conditions on $y = 0$:

$$\sigma_{yy} = \sigma_{xy} = 0 \quad \text{for } x \in [-a, a], \tag{1a}$$

$$\sigma_{yy} = \sigma_d(\delta) \quad \text{and} \quad \sigma_{xy} = 0 \qquad \text{for } |x| \in]a, a + d[\tag{1b}$$

and

$$\delta = \lim_{y \to 0} \left[u_y(x, y) - u_y(x, -y) \right], \tag{2}$$

where u_y is the displacement in the y-direction and $\delta|_{x=a} \equiv \delta_t$ is called the crack tip opening displacement (CTOD). Further,

$$u_y = 0 \quad \text{and} \quad \sigma_{xy} = 0 \qquad \text{for } |x| \in [a + d, \infty[.$$

The stress intensity factor is defined through

$$K_I = \lim_{x \to +0} \sqrt{2\pi x}\, \sigma_{yy}(x, 0), \tag{3}$$

where K_I is the mode I stress intensity factor. Upon employing the complex potential function $\Omega(z)$ for large $|z|$ [13], we can write

$$\sigma_{yy} + \sigma_{xy} = 4[\Omega'(z) + \Omega'(\bar{z})], \tag{4a}$$

$$\sigma_{yy} - i\sigma_{xy} = 2[\Omega'(z) + \Omega'(\bar{z}) + (z - \bar{z})\Omega''(\bar{z})], \tag{4b}$$

where the complex function $\Omega(z)$ is holomorphic in the whole plane cut through the crack line. In Eqs. (4a) and (4b), $z = x + iy$ with $i = \sqrt{-1}$, the prime denotes the derivative with respect to z, and the bar on top means the complex conjugate. It can be shown for the problem under consideration that K_I can be expressed as

$$K_I = \sigma_\infty \sqrt{\pi(a + d)} - \frac{1}{\sqrt{\pi a}} \times \left[\int_{-(a+d)}^{-a} \sigma_d \sqrt{\frac{a + x}{a - x}}\, dx - \int_a^{a+d} \sigma_d \sqrt{\frac{a + x}{a - x}}\, dx \right]. \tag{5}$$

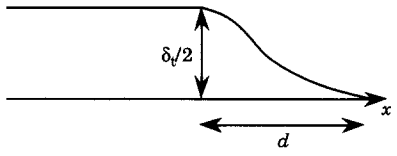

Fig. 2. Crack tip opening displacement δ_t.

Since the problem is symmetric about the y-axis, i.e., $\sigma_d(x) = \sigma_d(-x)$, Eq. (5) becomes

$$K_I = \sigma_\infty\sqrt{\pi(a+d)} - 2\frac{\sqrt{a+d}}{\pi}\int_a^{a+d} \times \frac{\sigma_d\,dx}{\sqrt{(a+d)^2 - x^2}}. \quad (6)$$

The CTOD for the geometry shown in Fig. 2 is [14]

$$\delta_t = 2u_y = \frac{\kappa+1}{4\mu}\sigma_\infty\sqrt{(a+d)^2 - a^2} - \frac{\kappa+1}{2\pi\mu}\int_x^{a+d}\frac{\eta\,d\eta}{\sqrt{\eta^2-a^2}}\int_a^{\eta}\frac{\sigma_{yy}\,d\xi}{\sqrt{\eta^2-\xi^2}}, \quad (7)$$

where

$$\kappa = \begin{cases} 3-4\nu, & \text{plane strain} \\ \dfrac{3-\nu}{1+\nu}, & \text{plane stress} \end{cases} \quad (8)$$

and

$$\mu = \frac{E}{2(1+\nu)}. \quad (9)$$

Here E is Young's modulus and ν Poisson's ratio.

2.1. The Dugdale zone

The simplest way to model the process region is to assume the magnitude of internal stresses is equal to the yield stress of material in that zone, i.e., we envision that fracture processes in the region d start at the onset of plastic deformation (the Dugdale zone) and that the continued fracture process occurs at a constant stress. Hence with $\sigma_d(x) = \text{constant} = \sigma_0$, where σ_0 is the yield stress, the integral term on right hand side of Eq. (6) gives the Dugdale zone stress intensity factor

$$K_I^D = -2\sqrt{\frac{a+d}{\pi}}\,\frac{\sigma_0}{1-2\nu}\arccos\left(\frac{a}{a+d}\right) \quad \text{(plane strain)}, \quad (10a)$$

$$K_I^D = -2\sqrt{\frac{a+d}{\pi}}\,\sigma_0\arccos\left(\frac{a}{a+d}\right) \quad \text{(plane stress)}. \quad (10b)$$

This quantity must balance the stress intensity factor induced by the remote tensile stress $K_\infty = \sigma_\infty\sqrt{\pi(a+d)}$ which yields

$$d = a\left[\sec\left(\frac{\pi\sigma_\infty(1-2\nu)}{2\sigma_0}\right) - 1\right] \quad \text{(plane strain)}, \quad (11a)$$

$$d = a\left[\sec\left(\frac{\pi\sigma_\infty}{2\sigma_0}\right) - 1\right] \quad \text{(plane stress)}. \quad (11b)$$

Using Eq. (7), the CTOD for this model is

$$\delta_t = \frac{8(1-\nu^2)}{\pi E}a\frac{\sigma_0}{(1-2\nu)}\ln\sec\left(\frac{\pi\sigma_\infty(1-2\nu)}{2\sigma_0}\right) \quad \text{(plane strain)}, \quad (12a)$$

$$\delta_t = \frac{8}{\pi E}a\sigma_0\ln\sec\left(\frac{\pi\sigma_\infty}{2\sigma_0}\right) \quad \text{(plane stress)}. \quad (12b)$$

Note that plane strain is obtained from plane stress by replacing $\sigma_0 \to \sigma_0/(1-2\nu)$ and $E \to E/(1-\nu^2)$.

2.2. Hydride stresses

When hydride is formed in Zircaloy a volume expansion around the zirconium hydride takes place. The stress inside the hydride can be calculated considering a representative simple geometry for hydride platelets. We assume, as in Shi and Puls [7], that the hydride has a rectangular shape shown in Fig. 3. Further, the local stress in the hydride is the sum of externally applied stress with no hydride present, σ^a, and a stress within the hydride, σ^h, generated by the hydride formation process in the absence of external forces, i.e., $\sigma_{loc} = \sigma^a + \sigma^h$.

When the hydride length is much larger than its thickness, i.e., $L/t \gg 1$ using the method of Chin [15], an analytical expression for σ^h can be obtained. Now by ignoring the free surface effects at the crack and assuming that there is only a non-zero initial strain $\varepsilon_{yy} = \varepsilon_\perp$, the analytical expression for σ^h is [7]

$$\sigma^h = \frac{-E\varepsilon_\perp}{2\pi(1-\nu^2)}\left[2\arctan\left(\frac{t}{2s}\right) - \frac{2s/t}{1+4s^2/t^2}\right], \quad (13)$$

where s is the distance from the front end of the hydride, at the crack tip, towards the center of the hydride.

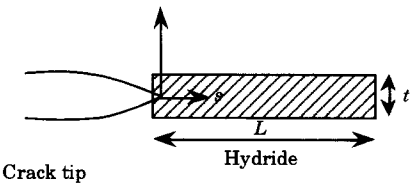

Fig. 3. Geometry of a hydride plate located at the crack tip.

For $s \gg t$ one can show

$$\sigma^{h} = -\frac{E\varepsilon_{\perp}}{4\pi(1-\nu^2)}\left(\frac{t}{s}\right), \quad s \gg t. \tag{14}$$

Numerical comparisons between Eqs. (13) and (14) reveal that the approximate expression in Eq. (14) is fair for $s \geq 0.3t$.

2.3. Fracture criterion

The aim is to determine at what level of applied stress the hydride will crack. We assume that the hydride cracks when

$$\sigma_{yy} + \sigma^{h} = \sigma_{f}^{h}, \tag{15}$$

where σ_{f}^{h} is the fracture stress for the hydride. Since the stress in the hydride for plane strain is $\sigma_{yy} = \sigma_0/(1-2\nu)$, utilizing Eqs. (13) and (15) we can write

$$\sigma_{loc} = \frac{\sigma_0}{1-2\nu} - \frac{E\varepsilon_{\perp}}{2\pi(1-\nu^2)}\left[2\arctan\left(\frac{t}{2s}\right) - \frac{2s/t}{1+4s^2/t^2}\right] = \sigma_{f}^{h}, \tag{16}$$

where $\sigma_{loc} = \sigma_{yy} + \sigma^{h}$ is the local stress in the hydride.

For $s \gg t$ Eq. (16) can be simplified as

$$\frac{\sigma_0}{1-2\nu} - \frac{E\varepsilon_{\perp}}{4\pi(1-\nu^2)}\frac{t}{s} = \sigma_{f}^{h}, \quad s \gg t \text{ (plane strain)}, \tag{17a}$$

and for plane stress we have

$$\sigma_0 - \frac{E\varepsilon_{\perp}}{4\pi}\frac{t}{s} = \sigma_{f}^{h}, \quad s \gg t \text{ (plane stress)}. \tag{17b}$$

One may re-express the hydride fracture criterion in terms of the stress intensity factors, that is to say, when K_I reaches a critical value K_{Ic} fracture will occur. The maximum local stress σ_{loc} occurs in our model at $s = d$ whereas for elastic–plastic material such as zirconium the Rice and Johnson's [16] analysis gives $s = 2\delta_t$ as the point where maximum stress occurs.

In sequel, confining our analysis to the region $s \gg t$ (see Fig. 3) Eq. (17a) gives

$$s = \frac{Et\varepsilon_{\perp}}{4\pi(1-\nu^2)\left[\sigma_0/(1-2\nu) - \sigma_{f}^{h}\right]}. \tag{18}$$

Letting $s = d$ and replacing σ_∞ with $K_{Ic}/\sqrt{\pi a}$

$$K_{Ic} = \frac{2\sigma_0\sqrt{\pi a}}{\pi(1-2\nu)} \arccos\left[1\Big/\left(1 + \frac{Et\varepsilon_{\perp}}{4\pi a(1-\nu^2)\left(\sigma_0/(1-2\nu) - \sigma_{f}^{h}\right)}\right)\right] \quad \text{for } s = d, \tag{19}$$

whereas setting $s = 2\delta_t$ with $\sigma_\infty = K_{Ic}/\sqrt{\pi a}$ yields

$$K_{Ic} = \frac{2\sigma_0\sqrt{\pi a}}{\pi(1-2\nu)} \arccos\left[\exp\left\{-E^2 t\varepsilon_{\perp}(1-2\nu)\Big/\left[64\sigma_0 a(1-\nu^2)\left(\frac{\sigma_0}{1-2\nu} - \sigma_{f}^{h}\right)\right]\right\}\right] \quad \text{for } s = 2\delta_t. \tag{20}$$

If $\sigma_\infty \ll \sigma_0$ Eqs. (19) and (20) can, respectively, be simplified to

$$K_{Ic}^2 \approx 2Et\varepsilon_{\perp}\sigma_0\Big/\left[\pi^2(1-\nu^2)\left(\frac{1}{1-2\nu} - \frac{\sigma_{f}^{h}}{\sigma_0}\right)(1-2\nu)^2\right] \quad \text{for } s = d \text{ and } \sigma_\infty \ll \sigma_0, \tag{21}$$

and

$$K_{Ic}^2 \approx E^2 t\varepsilon_{\perp}\left[8\pi(1-\nu^2)^2\left(\frac{1}{1-2\nu} - \frac{\sigma_{f}^{h}}{\sigma_0}\right)(1-2\nu)\right] \quad \text{for } s = 2\delta_t \text{ and } \sigma_\infty \ll \sigma_0. \tag{22}$$

Eqs. (19)–(22) apply to plane strain conditions. In Dugdale's plane stress formulation, Eqs. (19) and (20) are replaced as follows:

$$K_{Ic} = \frac{2\sigma_0\sqrt{\pi a}}{\pi} \arccos\left[1\Big/\left(1 + \frac{Et\varepsilon_{\perp}}{4\pi a\left(\sigma_0 - \sigma_{f}^{h}\right)}\right)\right] \quad \text{for } s = d, \tag{23}$$

and

$$K_{Ic} = \frac{2\sigma_0\sqrt{\pi a}}{\pi} \arccos\left[\exp\left\{-\frac{E^2 t\varepsilon_{\perp}}{64\sigma_0 a\left(\sigma_0 - \sigma_{f}^{h}\right)}\right\}\right] \quad \text{for } s = 2\delta_t. \tag{24}$$

If $\sigma_\infty \ll \sigma_0$, then Eqs. (21) and (22) can be written as

$$K_{Ic}^2 = 2Et\varepsilon_{\perp}\sigma_0\Big/\left[\pi^2\left(1 - \frac{\sigma_{f}^{h}}{\sigma_0}\right)\right] \quad \text{for } s = d, \ \sigma_\infty \ll \sigma_0, \tag{25}$$

$$K_{Ic}^2 = E^2 t\varepsilon_{\perp}\Big/\left[8\pi\left(1 - \frac{\sigma_{f}^{h}}{\sigma_0}\right)\right] \quad \text{for } s = 2\delta_t, \ \sigma_\infty \ll \sigma_0. \tag{26}$$

Table 1
Material data for Zr–2.5Nb [7] (T in K)

$E = 95900 - 57.4(T - 273)$ (MPa)
$\nu = 0.436 - 4.8 \times 10^{-4}(T - 300)$
$\varepsilon_{\perp} = 0.054$
$\sigma_0 = 1088 - 1.02T$ (MPa) unirradiated
$\sigma_0 = 1388 - 1.02T$ (MPa) irradiated
$\sigma_f^h = 7.357 \times 10^{-3} E$ (MPa)

Our motivation rests on the assumption that the fracture condition is best described as plane strain. However, the fracture process, i.e., microcracking, is understood to occur on several planes simultaneously. The irregular geometry of the hydride grains initiate microcracks perpendicular to the crack plane, thus locally relieving the tri-axial stress state.

2.4. Analysis

The stress intensity factor measured at different temperatures has been collected for Zr–2.5Nb by Shi and Puls [7]. The model presented here can be used to predict the temperature dependence of K_{Ic} using the data listed in Table 1 and a hydride thickness of $t = 2$ μm. In Fig. 4 we have plotted K_{Ic} for the approximate Dugdale-like model at $s = 2\delta_t$ and $s = d$ (Eqs. (25) and (26)) as a function of temperature. It can be seen that K_{Ic} increases with temperature until $\sigma_f^h \approx \sigma_0$ where Eqs. (25) and (26) became singular. Irradiation will reduce K_{Ic} as is expected. However, the model shows that the effect of temperature on K_{Ic} is insignificant or for that matter it gives an implausible result.

The associating exact expressions (Eqs. (23) and (24)) for $a = 60$ μm are plotted in Fig. 5. It is seen that for

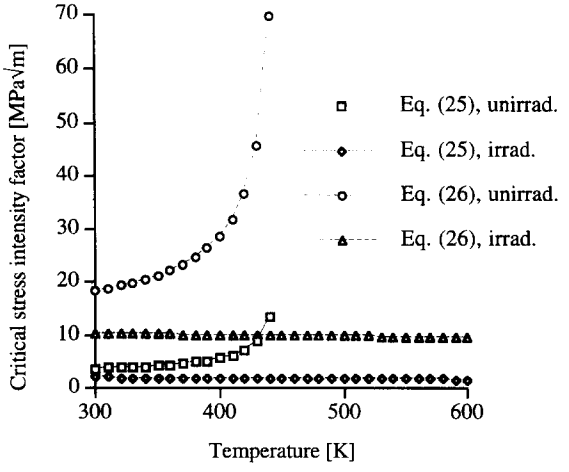

Fig. 4. Critical stress intensity factor in plane stress condition, using Eqs. (25) and (26) versus temperature for $\sigma_z \ll \sigma_0$.

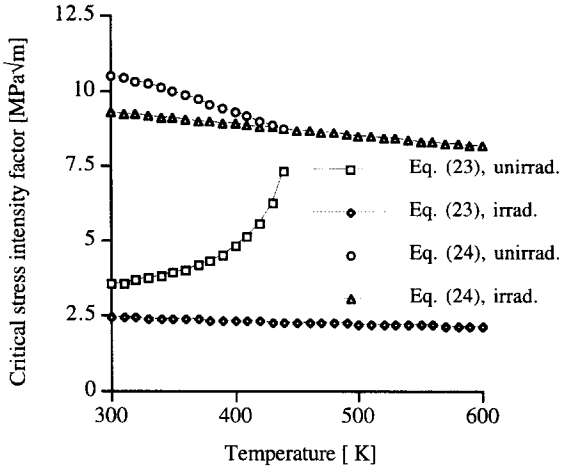

Fig. 5. Critical stress intensity factor using the exact solutions of the plane stress model (Eqs. (23) and (24)) versus temperature.

unirradiated material for $s = 2\delta_t$, K_{Ic} decreases with temperature, obviously a peculiar behavior, whereas for $s = d$ this temperature dependence is plausible.

The large values for K_{Ic} observed in the figures may be a reflection of the fact that at temperatures above 250°C the fracture process is moved from hydride phase to the matrix phase.

2.5. Model with mixed plane condition

The results obtained from the model presented in the preceding section did not satisfactorily describe the temperature dependence of the stress intensity factor in neither the plane stress or plane strain conditions. In this section we formulate the problem for a mixed plane condition, namely we assume that fracture occurs at the point $s = d$ (or $s = 2\delta_t$) in the plane stress state, whereas the stress in the process zone is considered to be in the plane strain condition. The critical stress intensity factors are hence derived to be

$$K_{Ic}\frac{2\sigma_0\sqrt{\pi a}}{\pi}\arccos\left[1\Big/\left(1+\frac{Et\varepsilon_{\perp}}{4\pi a(1-\nu^2)\left(\sigma_0/(1-2\nu)-\sigma_f^h\right)}\right)\right],$$

$$\text{for } s = d, \tag{27}$$

$$K_{Ic}^2 = \frac{2\sigma_0\sqrt{\pi a}}{\pi}\arccos\left[\exp\left\{-E^2 t\varepsilon_{\perp}\Big/\left[64\sigma_0 a(1-\nu^2)\left(\frac{\sigma_0}{1-2\nu}-\sigma_f^h\right)\right]\right\}\right],$$

$$\text{for } s = 2\delta_t. \tag{28}$$

In case of $\sigma_z \ll \sigma_0$, Eqs. (27) and (28) are approximated by

$$K_{Ic}^2 = 2Et\varepsilon_\perp \sigma_0 \Big/ \left[\pi^2(1-\nu^2)\left(\frac{1}{1-2\nu} - \frac{\sigma_f^h}{\sigma_0}\right)\right],$$

for $s = d$, (29)

$$K_{Ic}^2 = E^2 t\varepsilon_\perp \Big/ \left[8\pi(1-\nu^2)\left(\frac{1}{1-2\nu} - \frac{\sigma_f^h}{\sigma_0}\right)\right],$$

for $s = 2\delta_t$. (30)

2.6. Calculation results

Equations derived in the previous section for the mixed plane condition can be used to predict the temperature dependence of K_{Ic}. In Fig. 6 we present the result of calculations carried out by employing Eqs. (27) and (28) at $s = d$ and $s = 2\delta_t$, respectively, where we assumed $t = 2$ μm and the data in Table 1. The plots show tenable trends, i.e., K_{Ic} increases with temperature while neutron irradiation lowers K_{Ic} (only for $s = 2\delta_t$). The associating approximate relations Eqs. (29) and (30) offer values quite close to Fig. 6 and hence could alternatively be utilized.

We should note that $s = d$ does not satisfy the condition $s \gg t$ (for the obtained values of K_{Ic}), which was imposed to simplify the expression for the fracture stress of the hydride, and subsequently used in the derivations of the expressions for K_{Ic}. Similarly, this condition does not hold at $s = 2\delta_t$ for a large portion of the temperature interval. This implies an underestimation of K_{Ic}. One way

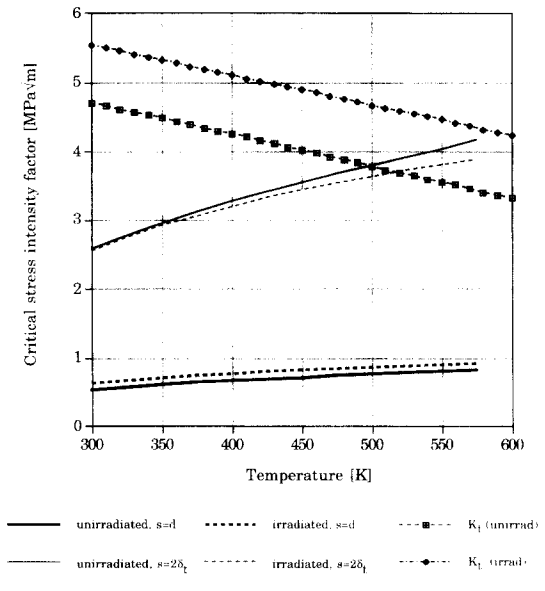

Fig. 6. Temperature dependence of the model with mixed plane conditions. $K_I = \sqrt{0.15E\sigma_0 t}$.

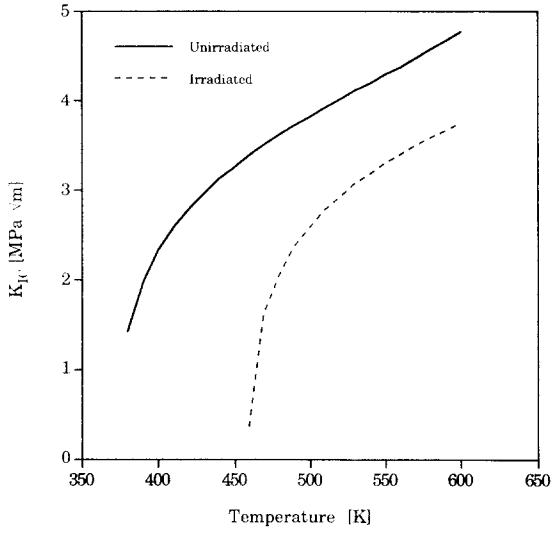

Fig. 7. Temperature dependence of critical stress intensity factor employing Eq. (32).

to consider this condition is to obtain the relation for σ^h for small s,

$$\sigma^h = \frac{-E\varepsilon_\perp}{2(1-\nu^2)(2\pi s/t + e^{-5.4s/t})} \quad (31)$$

If we employ Eq. (31) we obtain at $s = 2\delta_t$ the following expression for the critical stress intensity factor:

$$K_{Ic}^2 = E^2 t\varepsilon_\perp \Big/ \left[8\pi(1-\nu^2)\left(\frac{1}{1-2\nu} - \frac{\sigma_f^h}{\sigma_0}\right)\right] - \left(E\sigma_0 t e^{-10.8K_{Ic}^2/E\sigma_0 t}\right)/4\pi, \quad \text{at } s = 2\delta_t. \quad (32)$$

Eq. (32) is a transcendental equation for K_{Ic}^2 which may be expressed as

$$x = \mathscr{A} - \frac{e^{-10.8x}}{4\pi}, \quad (33)$$

where

$$x = \frac{K_{Ic}^2}{Et\sigma_0}, \quad (34)$$

$$\mathscr{A} = \left(\frac{E\varepsilon_\perp}{\sigma_0}\right) \Big/ \left[8\pi(1-\nu^2)\left(\frac{1}{1-2\nu} - \frac{\sigma_f^h}{\sigma_0}\right)\right]. \quad (35)$$

Eq. (33) has solutions for x provided $\mathscr{A} \geq 1/4\pi$. This implies that, using the data listed in Table 1, K_{Ic} can be determined for $T \gtrsim 380$ K for unirradiated and $T \gtrsim 460$ K irradiated material, respectively. Plots of K_{Ic} versus temperature are displayed in Fig. 7.

We should note that since Eqs. (28) and (30) are valid for $s \gg t$ ($s \gtrsim 0.3t$), they are applicable when

$$K_{Ic} \geq \sqrt{0.15E\sigma_0 t}, \quad (36)$$

where we have used $\delta_t \approx K_{Ic}^2/E\sigma_0$.

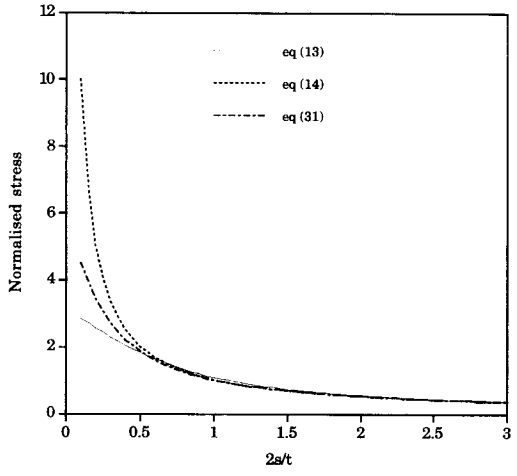

Fig. 8. Stress in the hydride platelet versus distance from the crack tip using different approximations. The normalized stress is $2(1-\nu^2)|\sigma^h|/E\varepsilon_\perp$.

To see the accuracy of the utilized approximations we have plotted $2(1-\nu^2)|\sigma^h|/E\varepsilon_\perp$ versus $2s/t$ as predicted by Eqs. (13), (14) and (31) in Fig. 8. It is seen that for $s \gtrsim 0.3t$ the three equations give the same results.

The results presented in Fig. 6 show that for irradiated and unirradiated materials, Eqs. (28) and (30) are accurate only for temperatures above 500 and 600 K, respectively, whereas Eq. (32) with the data in Table 1, is applicable to temperatures above 380 and 460 K for unirradiated and irradiated materials, respectively. The reason for this restriction could be due to the material property data (Table 1) used for the yield stress and Poisson's ratio. The applicable data should be for zirconium hydride in the considered zirconium alloy rather than for the matrix (Zr-alloy) properties. However, to our knowledge, such data are not available in literature. We expect the hydride yield stress to be lower than the yield stress value utilized here. A lower value for the yield stress somewhat increases the values for K_{Ic} and at the same time extends the validity of Eq. (32), thus eliminating the unphysical negative K_{Ic} region.

3. Multi-hydride platelets

A hydrided zirconium-based alloy comprises many hydride platelets. The formation of multi-layered hydrides at the front of the crack tip and uneven coverage of hydrides across and along the crack tip can affect the value of K_{Ic} considerably [7]. The critical stress intensity factor for multi hydride system may be written as

$$K_{IH} = fK_{Ic} + (1-f)K_{Ic}^{Zr}, \tag{37}$$

where K_{Ic}^{Zr} is the crack initiation threshold for a zirconium alloy containing no, or very low, area fraction of coverage

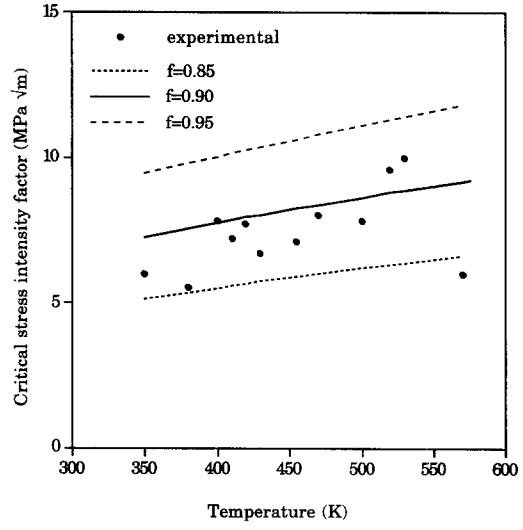

Fig. 9. Multi-hydride model (Eq. (37)) applied to Zr–2.5Nb with material properties given by Shi and Puls [7]. Critical stress intensity factor versus temperature for different hydride concentrations, where f is the area fraction of hydride coverage in the front of the crack tip.

of hydride platelets, f is the area fraction of hydride coverage in front of the crack tip, and K_{Ic} is the single platelet stress intensity factor discussed in the preceding sections. Experimental data obtained by Huang [17] indicate that

$$K_{Ic}^{Zr} = 30 + 0.045(T-300), \tag{38}$$

where T is the absolute temperature.

We have used Eqs. (30), (37) and (38) to predict K_{IH} as a function of temperature for Zr–2.5Nb for different values of f (Fig. 9). The experimental data [8] are also depicted in this figure. If Eq. (32) were used instead of Eq. (30), the agreement with experimental data would improve at lower temperatures.

3.1. Application to hydrides in Zircaloy

The model for the mixed plane condition presented in Section 2.4 is applied to hydrides in Zircaloy to predict the temperature dependence of the fracture toughness. The material property data used in this calculation is presented in Table 2. The fracture stress for hydride is assumed to be

Table 2
Material data for Zircaloy (T in K)

$E = 97800 - 58(T-273)$ (MPa) Zircaloy-2
$\nu = 0.436 - 2.48\times10^{-4}(T-298)$
$\sigma_0 = 803 - 0.652T$ (MPa) unirradiated, fully-annealed Zircaloy-2
$\sigma_0 = 1075 - 0.870T$ (MPa) irradiated, fully-annealed Zircaloy-2
$t = 2$ (μm)
$\varepsilon_\perp = 0.054$
$\sigma_f^h = 7.357\times10^{-3}[95900 - 57.4(T-273)]$ (MPa) Zr–2.5Nb

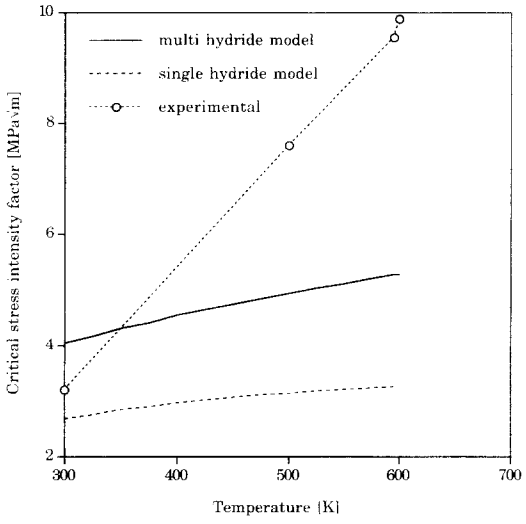

Fig. 10. Temperature dependence of the critical stress intensity factor K_{Ic} for irradiated and hydrided, fully annealed Zircaloy-2.

the same for Zircaloy and Zr–2.5Nb since in literature we could not find this value for Zircaloy.

Using Eqs. (30) and (37) with $f = 0.95$, and the data presented in Table 2, we have plotted K_{IH} as a function of temperature for both a single hydride and multi-hydrides in Zircaloy-2 in Fig. 10. In the same figure we have plotted three available experimental points [18]. It is noted that, although Eq. (30) is crude in the considered temperature range, the results are not totally inadequate. The increase in temperature of K_{IH} is quite weak compare with the experimental results, but this could be due to the unsatisfactory description of the temperature dependence of Poisson's ratio (Table 2). Also, there is a need for experimental data on yield stress and Poisson's ratio of the hydride in Zircaloy, as we discussed in the previous section.

4. Conclusion

In summary, we have applied the Dugdale model to calculate the critical stress intensity factor for the onset of crack propagation in hydrided Zr-alloys. Calculations performed for long hydrides located at both ends of a finite length crack show that for unirradiated material in plane stress condition, the critical stress intensity factor increases with temperature until the fracture stress becomes equal to the yield stress at which K_{Ic} becomes singular. For irradiated material K_{Ic} is a decreasing function of temperature which is an implausible result.

A mixed plane model where plane stress is assumed at $s = d$ (or $s = 2\delta_t$) while plane strain condition is considered in the process region offers a more plausible result than the former models, i.e., the critical stress intensity factor for both irradiated and unirradiated material (at $s = d$ and $s = 2\delta_t$) increases with temperature. However, the applicable equations are valid only for temperatures above 450 and 550 K for unirradiated and irradiated materials, respectively. We believe the main cause of these deficiencies in the model lies in the lack of appropriate experimental data to formulate adequate constitutive laws for hydride zirconium system. Nevertheless, the mixed plane theory has been applied to the case of multi hydride platelets. The agreement with experimental data (the critical stress intensity factor vs. temperature) on Zr–2.5Nb are satisfactory. For Zircaloy such data are not directly available. The model at best gives a conservative estimate (i.e., a lower bound) of the three data points available to us.

Our evaluation shows that for developing a mechanistic fracture criterion for hydrided Zircaloy, basic mechanical property data (constitutive relations) in the temperature range of interest (300 to 600 K) are sine qua non.

Acknowledgements

We are grateful to David Schrire and Sylvie Arsene for informative discussions. Special thanks go to Anette Medin for graphic assistance.

References

[1] C.E. Coleman, D. Hardie, J. Less-Common Met. 2 (1966) 168.
[2] I. Aitchison, in: Applications-related Phenomena in Zirconium and Its Alloys, ASTM-STP 458 (ASTM, Philadelphia, PA, 1969) p. 160.
[3] D.O. Northwood, U. Loassih, Int. Met. Rev. 28 (1983) 92.
[4] J.B. Bai, C. Prioul, J. Pelchat, F. Barcelo, in: Proc. Int. ANS/ENS Conf., Avignon, France, Apr. 21–24, 1991, p. 223.
[5] K.S. Chan, Acta Metall. Mater. 43 (1995) 4325.
[6] J.B. Bai, C. Prioul, D. Francois, Metall. Trans. A25 (1994) 1185.
[7] S.-Q. Shi, M.P. Puls, J. Nucl. Mater. 208 (1994) 232.
[8] L.A. Simpson, M.P. Puls, Metall. Trans. A10 (1979) 1979.
[9] M.F. Kanninen, C.H. Popelar, Advanced Fracture Mechanics (Oxford University, Oxford, 1985) ch. 5.
[10] T.M. Banks, A. Garlick, Eng. Fract. Mech. 19 (1984) 571.
[11] X.Q. Yuan, K. Tangri, J. Nucl. Mater. 105 (1982) 310.
[12] K.B. Broberg, Eng. Fract. Mech. 16 (1982) 497.
[13] A.E. Green, W. Zerna, Theoretical Elasticity (Dover, New York, 1992) ch. 8.
[14] I.N. Sneddon, M. Lowengrub, Crack Problems in the Classical Theory of Elasticity (Wiley, New York, 1969) ch. 2.
[15] Y.P. Chin, J. Appl. Mech. 44 (1977) 587.
[16] J.R. Rice, M.A. Johnson, in: Inelastic Behavior of Solids, eds. M.F. Kanninen, W.G. Adler, A.R. Rosenfield and R.I. Jaffee (McGraw-Hill, New York, 1970) p. 641.
[17] F.H. Huang, J. Nucl. Mater. 207 (1993) 103.
[18] D. Schrire, personal communication.